

A Simple Approach to Constraint-Aware Imitation Learning with Application to Autonomous Racing

Shengfan Cao, Eunhyek Joa, Francesco Borrelli

Abstract—Guaranteeing constraint satisfaction is challenging in imitation learning (IL), particularly in tasks that require operating near a system’s handling limits. Traditional IL methods often struggle to enforce constraints, leading to suboptimal performance in high-precision tasks. In this paper, we present a simple approach to incorporating safety into the IL objective. Through simulations, we empirically validate our approach on an autonomous racing task with both full-state and image feedback, demonstrating improved constraint satisfaction and greater consistency in task performance compared to a baseline method.

I. INTRODUCTION

Autonomous racing competitions, including the Indy Autonomous Challenge, FITENTH, and the DARPA Grand Challenge, drive innovation in high-speed control and real-time decision-making [1]. Traditional control strategies focus on optimal race-line generation but require extensive engineering and prior knowledge. Reinforcement learning (RL) can outperform human drivers in drone [13] and simulated vehicle racing [14], yet demands risky, large-scale training and struggles with sim-to-real transfer. Moreover, state-of-the-art platforms often rely on advanced sensors (e.g., LiDAR, D-GPS) and significant onboard computation, limiting deployment on low-cost systems. Consequently, developing efficient, learning-based control for resource-constrained hardware and limited sensing remains challenging.

Imitation Learning (IL), which has demonstrated success in robotics, autonomous vehicles, and gaming [2]–[4], emerges as a promising candidate to address these constraints. Recent advances in deep learning have further enhanced IL performance, allowing agents to mimic complex human strategies through the use of high-capacity models that map raw sensor data (e.g., images) to actions [11], [12].

Despite these successes, IL-based methods often overlook safety-critical aspects of decision-making. In many real-world scenarios, such as autonomous driving and drone navigation, the consequences of safety constraint violations can be severe. Purely maximizing imitation accuracy can lead to suboptimal or unsafe maneuvers, especially if the agent model has insufficient representation power to perfectly clone the expert demonstrations in all possible states. Consequently, ensuring that an IL agent respects safety constraints

(e.g., collision avoidance, maintaining certain system limits) remains an open and pressing challenge.

To address safety concerns, several recent efforts have attempted to augment IL with constraint satisfaction mechanisms. Many of these methods assume that the expert demonstrations themselves are safe or reliable, thereby focusing on identifying and prioritizing safety-critical states in the dataset [6], [18]. By emphasizing these states, the agent’s learned policy can allocate higher importance to correct behavior under dangerous conditions. SafeDagger [22] takes a different approach by training an additional classifier to predict deviations from the expert and switching to a backup policy when necessary. However, these approaches become less effective if the expert demonstrations are themselves risky or even contain unsafe actions. This gap highlights the need for a more robust framework that can handle unsafe expert trajectories while still aiming to learn a safe policy.

Parallel research in classical control has long studied the problem of safe control through approaches such as Model Predictive Control (MPC), Control Barrier Functions (CBFs), and Hamilton-Jacobi reachability analysis [7]–[10]. These methods provide rigorous guarantees about constraint satisfaction by, for example, constructing safe sets or using invariant sets to ensure that the system remains within specified limits. A common strategy involves the use of safety filters or shielding layers that modify the control commands if a safety violation is imminent [15]. Although such formal methods offer strong theoretical guarantees, they often scale poorly to high-dimensional, nonlinear systems. The computational overhead of solving online optimization problems or explicitly computing reachable sets becomes prohibitive in complex environments.

In this work, we address the problem of constraint-aware imitation learning under the realistic assumption that expert demonstrations may be unreliable or partially unsafe. Specifically, we aim to (1) learn a policy that mimics the behaviors from a set of expert demonstrations (some of which are failures) while avoiding constraint violation, and (2) develop a safety mechanism in the training pipeline that can handle image-based inputs and partial state observations.

Our main contributions are as follows:

- **Novel Implicit Safety Filter Architecture:** We propose a differentiable safety filter that can be embedded into classical imitation learning frameworks for high-dimensional, partially observed systems.
- **Data-driven Approximation of Safe Set:** We introduce a simple data-driven approach to approximate the safe set for constrained systems inspired by [7].

Shengfan Cao and Francesco Borrelli are with the Department of Mechanical Engineering, University of California at Berkeley, CA 94701 USA. Eunhyek Joa is with Zoox. The work is sponsored by the Department of the Navy, Office of Naval Research ONR N00014-24-2099. The content of the information does not necessarily reflect the position or the policy of the Government, and no official endorsement should be inferred.

- **Empirical Validation:** We demonstrate the effectiveness of our approach on high-dimensional, nonlinear, image-feedback systems, highlighting improvements in constraint satisfaction and consistency in task performance compared to baseline methods.

II. PROBLEM FORMULATION

A. System

Consider a nonlinear, time-invariant, deterministic, discrete-time system described as:

$$\begin{aligned} x_{k+1} &= f(x_k, u_k), \\ y_k &= h(x_k) + n_k, \end{aligned} \quad (1)$$

where x_k is the state, u_k is the control input, y_k is the measurement, and n_k is the measurement noise at time step k . The system is subject to constraints defined as:

$$x_k \in \mathcal{X}, u_k \in \mathcal{U}, \forall k \geq 0. \quad (2)$$

As a shorthand notation, we denote $\mathbf{u}_{0:N-1} = \{u_0, \dots, u_{N-1}\}$ as a control sequence. The state at time N resulting from applying the control sequence $\mathbf{u}_{0:N-1}$ to the system with dynamics f , initialized at the state x_0 , is denoted by $x_N = f(x_0, \mathbf{u}_{0:N-1})$, where each intermediate state is determined recursively with (1). We also denote a closed-loop trajectory by $\mathbf{x}_{0:N} = \{x_0, \dots, x_N\}$. This implies that there exists a feasible control sequence $\mathbf{u}_{0:N-1}$ such that $x_{k+1} = f(x_k, u_k)$ for all $k = 0, \dots, N-1$.

B. Constrained Optimal Control Task

In this paper, we consider the following constrained optimal control problem.

$$\begin{aligned} \min_{\mathbf{u}_{0:\infty}} \quad & \sum_{k=0}^{\infty} c(x_k, u_k) \\ \text{s.t.}, \quad & x_{k+1} = f(x_k, u_k), \\ & y_k = h(x_k) + n_k, \\ & x_k \in \mathcal{X}, u_k \in \mathcal{U}, \\ & \forall k \geq 0. \end{aligned} \quad (3)$$

where $c(\cdot, \cdot)$ is a cost function. We assume the existence of a zero-cost target set \mathcal{X}_f : once the system reaches \mathcal{X}_f , it can remain in the set at no further cost. Specifically, we use the following assumption on $c(\cdot, \cdot)$ and \mathcal{X}_f .

Assumption 1: (Non-negative Cost Function and Target Set) The cost function $c(x, u)$ is non-negative for all $x \in \mathcal{X}, u \in \mathcal{U}$. Moreover, $\forall x \in \mathcal{X}_f, \exists u \in \mathcal{U}, \text{s.t.}, f(x, u) \in \mathcal{X}_f, c(x, u) = 0$.

We determine whether a trajectory is successful by checking whether its terminal state reaches the target set, namely,

Definition 1: A closed-loop trajectory $\mathbf{x}_{0:N} = \{x_0, \dots, x_N\}$ is called **successful** if $x_N \in \mathcal{X}_f$, and **failed** if $x_N \notin \mathcal{X}_f$.

C. Safe Imitation Learning Problem

We are focused on the case where the controller only has access to the output y_k rather than direct access to x_k . Our objective is to design an output-feedback controller $\pi_\theta(y)$ that approximately solve (3). Assume we have access to a high-performing full-state feedback policy, denoted as $\pi_\beta(x)$, which acts as the expert. Our approach is to mimic $\pi_\beta(x)$ for designing the output feedback controller $\pi_\theta(y)$. Formally, this objective can be expressed as:

$$\begin{aligned} \min_{\theta} \quad & \mathbb{E}_{(x,y) \sim P((x,y)|\theta)} [\mathcal{L}(\pi_\theta(y), \pi_\beta(x))], \\ \text{s.t.} \quad & f(x, \pi_\theta(y)) \in \mathcal{R}_\infty^B(\mathcal{X}_f), \end{aligned} \quad (4)$$

where $P((x,y)|\theta)$ denotes the distribution of state-output pairs induced by π_θ , $\mathcal{L}(\cdot, \cdot)$ is a measurement of the discrepancy between two actions, and $\mathcal{R}_\infty^B(\mathcal{X}_f)$ is a backward reachable tube from the target set \mathcal{X}_f , which is defined as follows.

Definition 2 (Backward Reachable Tube): The N -step backward reachable tube $\mathcal{R}_N^B(\mathcal{S})$ is a set of states $x_0 \in \mathcal{X}$ that can be driven into a set \mathcal{S} in N time steps without constraint violation. Formally,

$$\mathcal{R}_N^B(\mathcal{S}) = \left\{ x_0 \mid \exists \mathbf{u}_{0:N-1}, \text{s.t.} \begin{aligned} & f(x_0, \mathbf{u}_{0:N-1}) \in \mathcal{S}, \\ & x_0 \in \mathcal{X}, \forall k < N, \\ & u_k \in \mathcal{U}, \forall k < N. \end{aligned} \right\}. \quad (5)$$

If $N \rightarrow \infty$, we refer to \mathcal{R}_∞^B as the infinite-time backward reachable tube.

Remark 1: Per Assumption 1, $\mathcal{R}_N^B(\mathcal{X}_f) \subseteq \mathcal{R}_\infty^B(\mathcal{X}_f), \forall N$.

Definition 3 (Safety): We will refer to states in the infinite-time backward reachable tube as **safe** states, as there exists some policy that drives the system into the target set from those states.

Deriving the backward reachable tube $\mathcal{R}_\infty^B(\mathcal{X}_f)$ is non-trivial, which poses a challenge in solving (4). In practice, the safety constraint is often neglected by assuming the cloning can be sufficiently accurate and the expert is reliable and robust [21]. However, in applications such as autonomous racing, achieving high performance requires policies to push systems to limits. Any deviation by the learned policy π_θ from expert demonstrations, especially in unsafe directions, risks losing recursive feasibility and causing constraint violations. Thus, prioritizing a safe operating policy over perfect-expert

cloning becomes essential.

In the following section, we describe how previous research tackles this challenge and their limitations. Then, in section IV, we present our approach to solving (4).

III. RELATED WORK

A. Behavior Cloning

One naive objective of behavior cloning is to find θ that minimizes the discrepancy between its actions and those of

the expert in ℓ_2 distance.

$$\theta_{\text{naive}}^* = \arg \min_{\theta} \mathbb{E}_{(x,y) \sim P((x,y)|\theta)} \underbrace{\left[\|\pi_{\theta}(y) - \pi_{\beta}(x)\|^2 \right]}_{\mathcal{L}_{\text{clone}}}. \quad (6)$$

Let the imitation learning policy be denoted as:

$$\pi_{\text{IL}}(\cdot) = \pi_{\theta_{\text{naive}}^*}(\cdot) \quad (7)$$

In applications like self-driving cars [19] and manipulation [20], many variations of behavior cloning use (6) as the fundamental building block, and add additional tunable loss terms to achieve better performance on specific tasks.

Behavior cloning is effective in mimicking expert demonstrations in situations well-represented in its training data, but usually generalizes poorly to novel states, which is known as covariate shift [21]. Dataset Aggregation (DAGGER) [17] is an effective interactive online learning framework that mitigates this problem by collecting on-policy rollouts and use the expert to relabel the data set. However, DAGGER's on-policy training requires costly hardware data collection. In addition, the theoretical zero regret promise is only achieved asymptotically, necessitating many epochs for accurate cloning. Models with limited representational power may not achieve zero loss even theoretically.

Another significant shortcoming of (6) is its ignorance of constraints and lack of direction-specific penalties. Prior to achieving perfect behavior cloning (if it is even feasible), it is essential to ensure that the discrepancy is less likely in unsafe directions.

B. Formal Methods for Constraint Satisfaction

To achieve constraint satisfaction, common approaches in the control community include safety filters and reference governors [8], [23].

Safety filters are typically additional modules designed independently from the controller, and are placed between the controller and the system to project unsafe actions into a pre-designed safe set. This allows a high-performing policy learned within safety-ignorant frameworks like reinforcement learning to operate safely on a physical system [15].

Let $\hat{u}_k = \pi_{\text{IL}}(y_k)$ be an output-feedback policy trained to minimize the naive ℓ_2 imitation loss in (6), which produces potentially unsafe actions. We want to apply a safety filter π_{SF} after π_{IL} to enforce constraint satisfaction. A straightforward implementation is the minimum-effort predictive safety filter [15], which iteratively solves the problem in (8) and applies the first input in the optimal action sequence.

$$\begin{aligned} \min_{\mathbf{u}_{0:N-1|k}} \quad & \|u_{0|k} - \hat{u}_k\|_2^2, \\ \text{s.t.} \quad & x_{i+1|k} = f(x_{i|k}, u_{i|k}), \\ & x_{0|k} = x_k, \quad x_{i|k} \in \mathcal{X}, \quad u_{i|k} \in \mathcal{U}, \\ & x_{N|k} \in \mathcal{R}_{\infty}^B(\mathcal{X}_f), \\ & \forall i = 0, \dots, N-1. \end{aligned} \quad (8)$$

where N is the horizon of the predictive safety filter and $u_{i|k}$ and $x_{i|k}$ are the input and the predicted state at time

step $k+i$, respectively. After solving (8), the optimal safety filter policy

$$u_k = \pi_{\text{SF}}(\hat{u}_k | x_k) = u_{0|k}^* \quad (9)$$

is applied to the system (1). Note that (8) relies on full-state feedback.

Other variations of safety filters are formulated based on formal methods such as CBF [24], [25], Hamilton-Jacobi reachability analysis [9], but their overarching goal is similar to (8).

Reference governors [8], on the other hand, approach the problem by proactively modifying the reference signal before it reaches the controller to ensure the system closely follows the reference without violating the constraints.

However, most existing formal methods for constraint satisfaction assume that full-state information is available or can be estimated accurately. Many real-world applications operate primarily on high-dimensional sensor data (e.g., camera images), and extending safety filters to operate directly in an image-based or partial-observation setting is an outstanding challenge.

IV. PROPOSED APPROACH: CONSTRAINT-AWARE BEHAVIOR CLONING

In this section, we present a constraint-aware imitation learning framework to approximately solve (4). Given an expert policy $\pi_{\beta}(x)$, we incorporate the safety filter (8) into behavior cloning (6), formulating output-feedback policies $\pi_{\theta}(y)$ that leverage the filter as an additional training-time expert. Specifically, we aim to directly recover

$$\theta_{\text{CA}}^* = \arg \min_{\theta} \mathbb{E}_{(x,y) \sim P((x,y)|\theta)} \underbrace{\left[\mathcal{L}(\pi_{\theta}(y), \pi_{\text{SF}}(\pi_{\text{IL}}(y) | x)) \right]}_{\mathcal{L}_{\text{CA}}} \quad (10)$$

from privileged end-to-end training, which aims to achieve both high performance and constraint satisfaction. In the scope of this paper, we use the naive behavior cloning objective in (6) and the min-effort predictive safety filter in (8) as an example to facilitate analysis.

A. Construction of \mathcal{L}_{CA}

In this section, we discuss the construction of \mathcal{L}_{CA} in (10). As a first step, we approximately reformulate (8) to make it differentiable, enabling its use in backpropagation. Let $N=1$ for the safety filter formulated in (8). With Definition 2, the constraints in (8) can be written as:

$$f(x_k, u_{0|k}) \in \mathcal{R}_{\infty}^B(\mathcal{X}_f). \quad (11)$$

The minimum effort safety filter π_{SF} in (8) can be approximated by π_{ξ} by softening the constraint.

$$\begin{aligned} \pi_{\xi}(\hat{u}_k | x_k) \triangleq \arg \min_{u_{0|k} \in \mathcal{U}} \left[\|u_{0|k} - \hat{u}_k\|^2 \right. \\ \left. + \mathbb{I}_{\mathcal{R}_{\infty}^B(\mathcal{X}_f)}(f(x_k, u_{0|k})) \right], \end{aligned} \quad (12)$$

where \mathbb{I} is implemented as a soft indicator function

$$\mathbb{I}_{\mathcal{R}_{\infty}^B(\mathcal{X}_f)}(x) = -\lambda \log p(x \in \mathcal{R}_{\infty}^B(\mathcal{X}_f)), \quad (13)$$

and $\lambda > 0$ is a hyperparameter. Note that if the classifier p is a hard classifier that always correctly outputs 0 for unsafe or 1 for safe, (13) strictly enforces safety.

Suppose $p(x \in \mathcal{R}_\infty^B(\mathcal{X}_f))$ is given as a differentiable function. Then, $\pi_\xi(\hat{u}_k | x_k)$ in (12)-(13) can be numerically approximated with gradient-based methods.

Next, we seek to integrate (6) and (12) into a joint objective \mathcal{L}_{CA} . In this step, we use the following assumption.

Assumption 2 (Zero-bias training of π_{IL}): To facilitate derivation of \mathcal{L}_{CA} , we assume the naive behavior cloning policy π_{IL} clones the expert policy π_β with no bias on the training set \mathcal{D} , i.e., $\mathbb{E}_{(x,y) \sim \mathcal{D}}[\pi_{IL}(y) - \pi_\beta(x)] = 0$. Additionally, assume the dataset \mathcal{D} has no distribution shift from the task.

Plug $\hat{u}_k = \pi_{IL}(y)$ and (12) into (10),

$$\begin{aligned} \theta_{CA}^* &= \arg \min_{\theta} \mathbb{E}_{(x,y) \sim P((x,y)|\theta)} \left[\|\pi_\theta(y) - \pi_{IL}(y)\|_2^2 \right. \\ &\quad \left. - \lambda \log p(f(x, \pi_\theta(y)) \in \mathcal{R}_\infty^B(\mathcal{X}_f)) \right] \\ &= \arg \min_{\theta} \left[\underbrace{\|\pi_\theta(y) - \pi_\beta(x)\|_2^2}_{\mathcal{L}_{\text{clone}}} \right. \\ &\quad \left. - \lambda \log p(f(x, \pi_\theta(y)) \in \mathcal{R}_\infty^B(\mathcal{X}_f)) \right]. \end{aligned} \quad (14)$$

(14) is the joint objective \mathcal{L}_{CA} of the naive behavior cloning agent π_{IL} and the safety filter π_{SF} . Note that (14) contains the naive behavior cloning loss $\mathcal{L}_{\text{clone}}$, same as in (6), and an additional NLL loss $\mathcal{L}_{\text{safety}}$. This can be considered as concurrently learning from two experts, one that optimizes performance and one that enforces constraint satisfaction. We refer to the expert providing $\mathcal{L}_{\text{safety}}$ as the **safety critic**.

B. Tractable Reformulation of $\mathcal{L}_{\text{safety}}$

The safety critic consists of two components: the forward dynamics $f(x, u)$, and the safety likelihood $p(x \in \mathcal{R}_\infty^B(\mathcal{X}_f))$, both assumed to be unknown.

We use the learned function approximators $\hat{f}_{\phi_f}(x, u)$ and $\hat{p}_{\phi_p}(x)$ as their corresponding surrogates. Specifically, the forward dynamics estimator \hat{f}_{ϕ_f} is trained via auto-regression, i.e.,

$$\phi_f^* = \arg \min_{\phi_f} \mathbb{E}_{(x,u,x') \sim \mathcal{D}} [\|x' - \hat{f}_{\phi_f}(x, u)\|^2]. \quad (15)$$

The safety likelihood estimator \hat{p}_{ϕ_p} is learned using the binary cross-entropy loss, i.e.,

$$\phi_p^* = \arg \max_{\phi_p} \mathbb{E}_{x \sim \mathcal{D}} \left[\left(s \log \hat{p}_{\phi_p}(x) + (1-s) \log(1 - \hat{p}_{\phi_p}(x)) \right) \right], \quad (16)$$

where

$$s = \begin{cases} 1, & x \in \mathcal{R}_\infty^B(\mathcal{X}_f), \\ 0, & x \notin \mathcal{R}_\infty^B(\mathcal{X}_f). \end{cases} \quad (17)$$

However, computing s is challenging due to unknown $\mathcal{R}_\infty^B(\mathcal{X}_f)$, which is difficult to compute.¹ Next we present a simple self-supervised approach to acquire surrogate labels s to learn \hat{p}_{ϕ_p} from closed-loop trajectories without any knowledge of the system, called **safety auto-labeling**.

Let $\mathcal{D} = \{\mathbf{x}_{0:T_j}^{(j)}\}$ be a dataset collected by rolling out a data collection policy π_{collect} in closed-loop from various initial states, where j is the index of the trajectory in the dataset. Assume π_{collect} is designed such that it can generate both successful and failed iterations.

Recall Definition 1 for successful and failed trajectories. The dataset \mathcal{D} can be partitioned into $\mathcal{D}_+ = \{\mathbf{x}_{0:T_j}^{(j)} | x_{T_j}^{(j)} \in \mathcal{X}_f\}$ and $\mathcal{D}_? = \{\mathbf{x}_{0:T_j}^{(j)} | x_{T_j}^{(j)} \notin \mathcal{X}_f\}$.

By Definition 2, all states visited during successful iterations are safe, i.e.,

$$\mathcal{D}_+ \subseteq \mathcal{R}_\infty^B(\mathcal{X}_f). \quad (18)$$

As its counterpart, ideally we want $\mathcal{D}_- \subseteq \overline{\mathcal{R}_\infty^B(\mathcal{X}_f)}$ to construct the loss in (16). However, states in $\mathcal{D}_?$, visited during failed iterations, are not necessarily unsafe.

Proposition 1: Suppose \mathcal{R} is a set of interest, and we have a set of samples \mathcal{S} from \mathcal{R} . Let $B_\rho(x)$ be a ball with radius ρ , centered at x , and $\text{conv}(\cdot)$ be the convex hull of a set. If $x \in \text{conv}(\mathcal{S} \cap B_\rho(x))$, then $d(x, \partial\mathcal{R}) \geq -\rho$, where

$$d(x, \partial\mathcal{R}) = \begin{cases} \inf_{y \in \partial\mathcal{R}} \|x - y\|, & \text{if } x \in \mathcal{R}, \\ -\inf_{y \in \partial\mathcal{R}} \|x - y\|, & \text{if } x \notin \mathcal{R}. \end{cases}$$

If, in addition, \mathcal{R} is locally convex at x within radius ρ , then $d(x, \partial\mathcal{R}) \geq 0$.

Let

$$\mathcal{D}_- \triangleq \mathcal{D}_? \setminus \{x \in \mathcal{D}_? | x \in \text{conv}(\mathcal{D}_+ \cap B_\rho(x))\}. \quad (19)$$

Proposition 1 indicates that by excluding points that are in the convex hull of states known to be safe, \mathcal{D}_- contains only states that are likely unsafe with higher confidence, and thereby reducing false negatives in the binary labels.

Figure 1 illustrates an example of the proposed auto-labeling technique and its effect on binary safety classification. With \mathcal{D}_+ sufficiently covering $\mathcal{R}_\infty^B(\mathcal{X}_f)$, and $\mathcal{D}_?$ sufficiently covering \mathcal{X} , the decision boundary $\hat{p} = 0.5$ closely aligns with its true boundary, particularly when ρ is appropriately small. As long as the set remains locally convex within a radius of ρ , the method correctly identifies points inside $\mathcal{R}_\infty^B(\mathcal{X}_f)$ from $\mathcal{D}_?$.

Without assuming the local convexity property, the choice of ρ is critical. Note that in the example, the true set boundary is concave with a sharp corner. In an online iterative learning framework, ρ should adapt to the sample density of \mathcal{D}_+ , decreasing as density increases. A large ρ may over-smooth concave boundaries, while a small ρ risks false negatives for not getting sufficient neighbors for

¹For low-dimensional linear systems, the backward reachable tube can be computed numerically [26]. The safety of individual states can also be approximated using the feasibility of an MPC controller with perfect modeling of the dynamics and the constraints [15]. However, it is generally a challenge to compute $\mathcal{R}_\infty^B(\mathcal{X}_f)$ for a black-box, high-dimensional, nonlinear system.

comparisons, affecting classification stability. Dynamically decreasing ρ as sample density of \mathcal{D}_+ increases enables \hat{p} to first capture the macroscopic structure of $\mathcal{R}_\infty^B(\mathcal{X}_f)$ before refining finer details. Note that the proposed local convex hull-based safety boundary estimation can be extended to account for different types of uncertainty by incorporating robustified convex hull approximations.

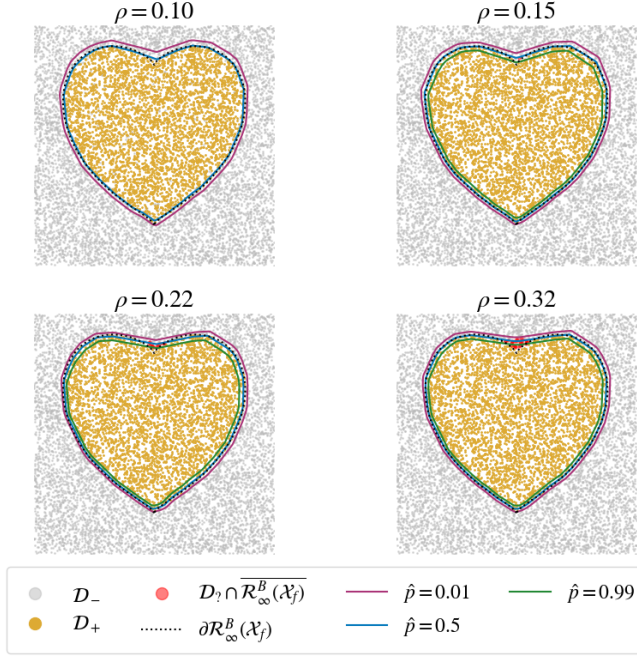


Fig. 1: Illustration of the proposed safety auto-labeling algorithm and the corresponding decision boundary in a constructed example. The **dotted black curve** is the true boundary of $\mathcal{R}_\infty^B(\mathcal{X}_f)$. ρ 's are the radius of the nearest neighbor in Alg. 1. \mathcal{D}_+ is uniformly sampled from $\mathcal{R}_\infty^B(\mathcal{X}_f)$, and $\mathcal{D}_?$ is uniformly sampled from $\mathcal{X} \supset \mathcal{X}_f$. The **blue curve** is the decision boundary of an MLP as a binary classifier trained to classify states in \mathcal{D}_+ and \mathcal{D}_- , and the **purple and green curves** are its level curves of higher confidence. **Red points** are states incorrectly filtered from $\mathcal{D}_?$. Note that as ρ decreases, less points are incorrectly removed from $\mathcal{D}_?$ in the concave regions, resulting in a better estimation of the true boundary in those regions.

C. Proposed learning framework

The proposed learning framework is described in Algorithm 1. This framework builds upon DAGger by incorporating the training of \hat{f}_{ϕ_f} and \hat{p}_{ϕ_p} into the process, and incorporating the necessary auto-labeling process for their training.

V. EXPERIMENTS

This section presents the empirical results of the proposed learning framework.² We apply our approach in a CARLA-

²An implementation of the experiments in this paper can be found at <https://github.com/CadenzaCoda/ConstraintAwareIL.git>.

Algorithm 1 Constraint-aware Behavior Cloning

```

Initialize  $\mathcal{D}_+, \mathcal{D}_?$  as empty sets
Appropriately initialize  $\theta, \phi_f, \phi_p$ 
for  $j \leftarrow 0, \dots, M - 1$  do
     $\pi_{\text{collect}} \leftarrow \alpha^j \pi_\beta + (1 - \alpha^j) \pi_\theta \triangleright \alpha$  is a hyperparameter
    Rollout  $\pi_{\text{collect}}$  to collect  $\mathcal{D}_{\text{new}}$ 
    Partition  $\mathcal{D}_{\text{new}}$  into  $\mathcal{D}'_+$  and  $\mathcal{D}'_?$ 
     $\mathcal{D}_+ \leftarrow \mathcal{D}_+ \cup \mathcal{D}'_+$ 
     $\mathcal{D}_? \leftarrow \mathcal{D}_? \cup \mathcal{D}'_?$ 
    for  $x \in \mathcal{D}_?$  do  $\triangleright$  Safety auto-labeling.
         $\mathcal{S} \leftarrow \text{RadiusNeighbors}(x \mid \mathcal{D}_+, \rho)$ 
        if  $x \in \text{GetConvexHull}(\mathcal{S})$  then
            Remove  $x$  from  $\mathcal{D}_?$   $\triangleright$  Remove if likely safe.
        end if
    end for
    ComputeGradient( $\mathcal{D}_+, \mathcal{D}_? \mid \pi_\theta, \hat{f}_{\phi_f}, \hat{p}_{\phi_p}$ )  $\triangleright$  See Fig. 2
    if  $j \bmod k_f = 0$  then  $\triangleright k_f = 5$  in our impl.
         $\phi_f \leftarrow \text{Update}(\phi_f \mid \nabla_{\phi_f} L_{\text{dyn}})$ 
    end if
    if  $j \bmod k_p = 0$  then  $\triangleright k_p = 10$  in our impl.
         $\phi_p \leftarrow \text{Update}(\phi_p \mid \nabla_{\phi_p} L_{\text{critic}})$ 
    end if
     $\theta \leftarrow \text{Update}(\theta \mid \nabla_\theta L_{\text{agent}})$ 
end for

```

based autonomous racing simulation [27] with customized vehicle dynamics. The state x in the experiments is modeled as $x = [v_{\text{long}} \ v_{\text{tran}} \ \omega_\psi \ s \ x_{\text{tran}} \ e_\psi]^T$, capturing the position and velocity of the rigid body in the Frenet frame. The inputs are $u = [u_a \ u_{\text{steer}}]^T$, corresponding to the throttle and steering control of the car. The output y consists of an RGB image from a front-facing camera and velocity measurements, i.e., $y = [\text{Img}(x) \ v_{\text{long}} \ v_{\text{tran}} \ \omega_\psi]$. These output feedback signals are assumed to be available because they can also be readily obtained on a physical platform equipped with a camera, an IMU, and wheel encoders.

Fig. 3 shows an example of the first-person camera view and the top view of the race track. Note that the direction of the sunlight is randomized with each environment reset. We further assume the image contains no distinguishable landmark to uniquely determine the location of the ego vehicle. The ground truth vehicle dynamics in the simulator is treated as a black box non-linear system in the training pipeline.

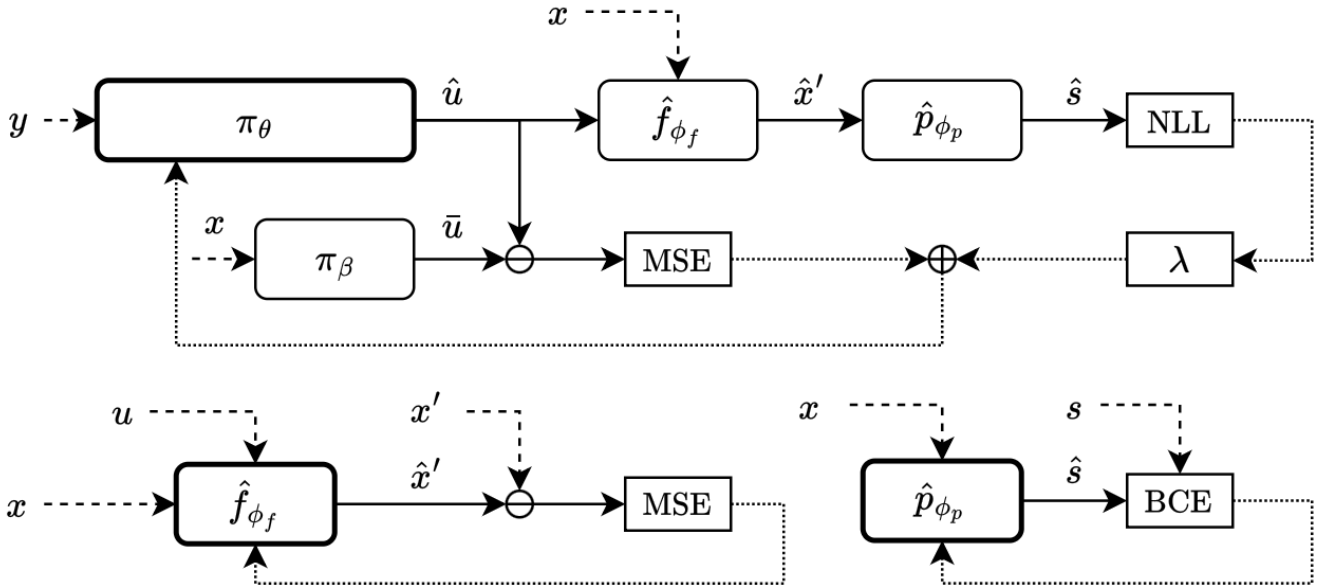


Fig. 2: Gradient Computation in the Proposed Architecture. **Dashed lines** represent inputs from the dataset \mathcal{D} , where each entry consists of state x , system output y , safety label s , closed-loop action u , and next state x' . Inputs from the dataset are always selected with the same index. **Dotted lines** indicate the correspondence between each loss function and its target module. **Bold-faced blocks** indicate trainable modules, while non-bold blocks remain frozen during training. **Rectangular blocks** represent loss functions: MSE (mean squared error), NLL (negative log-likelihood), and BCE (binary cross-entropy). During test time, only the policy network π_θ is used, while all other modules participate solely in training.

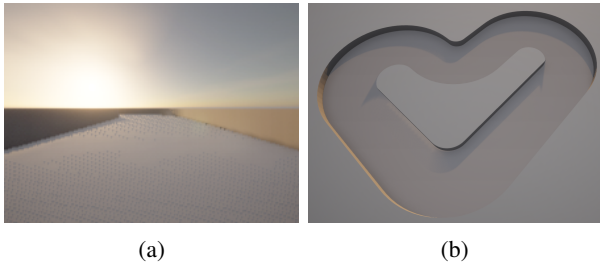


Fig. 3: The CARLA-based simulation environment for the experiments. **Left:** Example of onboard front-facing camera view $\text{Img}(x)$. **Right:** Geometry of the race track in the experiments.

Note that we utilize the **early stopping (ES)** technique to stop the training when the evaluation performance is at its peak. This is a common technique in machine learning to avoid overfitting to the measurement noise, causing the performance to degrade. The early stopping condition in our implementation is when the controller completes 50 consecutive laps for the second time.

Also, as a baseline for our approach in all experiments, we choose the naive behavior cloning objective in (6) and the DAgger framework to train a policy with the same architecture.

A. Image Feedback Autonomous Path Following

We first apply our method to learn to follow the track at a conservative speed. The expert $\pi_\beta(x)$ is a PID controller,

tuned to track the center line at 1 m/s. The policy $\pi_\theta(y)$ has access to image and velocity measurements. The architecture of $\pi_\theta(y)$ is based on ResNet18, with the final linear layer replaced with a three-layer MLP with 128 hidden neurons.

Figure 4 compares the proposed method with the baseline. As shown, both approaches lead to a policy that can complete 50 consecutive laps. However, the proposed method achieved this with fewer training epochs.

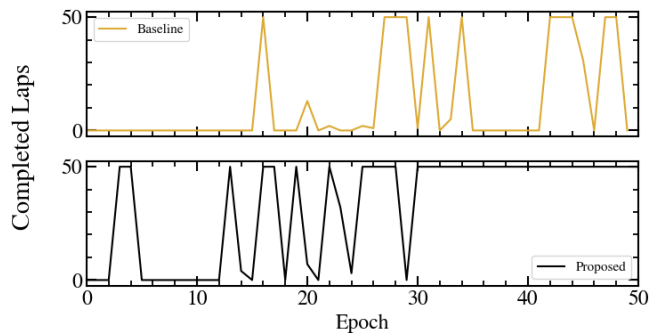


Fig. 4: Comparison between the baseline and the proposed method in Experiment V-A. The x-axis is the number of training epochs and the y-axis is the successful iterations completed without constraint violation. The tests are initialized at the same initial condition and are truncated once the controller completes 50 laps. In the proposed method, $\lambda = 1$, $\rho = 1$.

B. Full-state Feedback Autonomous Car Racing

Next, we apply our approach to an autonomous car racing task. In only this example, we allow the policy to observe the full state.

The objective of the task is to continuously complete as many consecutive laps as possible with minimum lap time while avoiding collision with the boundary of the track. The expert policy π_β is designed to achieve strong performance while adhering to constraints, often operating near the limits of the system. The architecture of policy π_θ in this experiment is restricted to 3-layer MLPs with 128 hidden neurons.

Fig. 5 and 6 show the comparison between the proposed and baseline method in the test time performance.

Precision is key in this task, as we observed constraint violation can be caused by small deviations from the expert demonstrations at critical moments, such as when making a tight turn at high speed. Without safety-specific penalty in the learning objective, it takes extreme behavior cloning precision, and consequently, many training epochs, to consistently avoid constraint violation. This poses a significant challenge especially if π_β is not robust to large input disturbance.

In contrast, our approach effectively reduced the likelihood of unsafe deviation from the expert, therefore leading to higher overall return with less training effort. Additionally, our approach led to similar average lap time but lower time variability, compared to the baseline and the expert, indicating improved consistency of the learned policy.

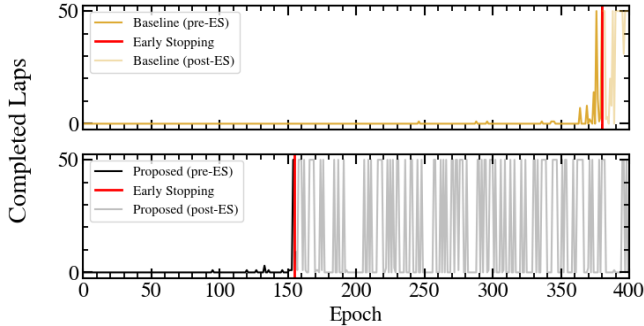


Fig. 5: Comparison of evaluation performance between the baseline and the proposed method in Experiment V-B. The x-axis is the number of epochs, and the y-axis is the successful iterations completed without constraint violation. The tests are initialized at the same initial condition and are truncated once the controller completes 50 laps. **Early stopping** is applied when a controller completes 50 laps for the second time. In the proposed method, $\lambda = 10$, $\rho = 1$.

C. Image-feedback Autonomous Car Racing

Next, we explore the task with the same setup and objective described in V-B, but the policy can only observe the output of the system. The architecture of π_θ is based on ResNet18, with the final linear layer replaced with a 3-layer MLP with 128 hidden neurons.

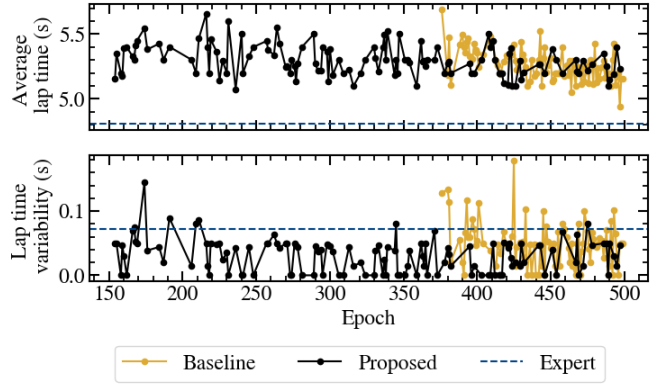


Fig. 6: Lap time and average and variability of the baseline and the proposed imitation learning objective in Experiment V-B. The variability is characterized by the standard deviation of lap times. The plot only shows epochs where the controller completes 50 laps. The dashed line shows the statistics of π_β .

Fig.7a compares the performance of the proposed method against the baseline. The proposed method successfully recovered a policy capable of completing 50 consecutive laps within 80 epochs, whereas the baseline failed to exceed even 10 laps. Fig.7b illustrates the rollout trajectory of π_θ when early stopping occurs at epoch 81. The trajectory indicates that π_θ learned to maintain a safe distance from walls while achieving consistent lap times.

The partial observability and the sensor noise made this task particularly challenging, and we observed particularly high variability in training dynamics in this case. However, we found an overall reduced failure rate and improved consistency across iterations in multiple repetitions with various hyper-parameter settings.

In addition, we repeatedly noticed a spike in test time performance at around 100 epochs. Considering the challenge imposed by partial observability and noise, we suggest applying early stopping when the performance is at its peak, rather than continuing training in the hope that the performance will further improve.

VI. DISCUSSION AND FUTURE WORK

In this work, we introduced a learned safety penalty into the imitation learning objective to address safety-critical tasks. Our experimental results demonstrate that this addition substantially reduces constraint violation rates and stabilizes performance, particularly during the earlier stages of training. Moreover, we empirically showed the effectiveness of the approach in vision-based end-to-end learning tasks. Notably, our method also achieves safe policy recovery in tasks requiring operation near the system’s handling limits, a setting where traditional imitation learning often struggles.

For future work, we plan to extend the proposed approach to other imitation learning objectives and safety filters for improved performance. Additionally, we aim to address the high-variance training dynamics caused by the non-stationary

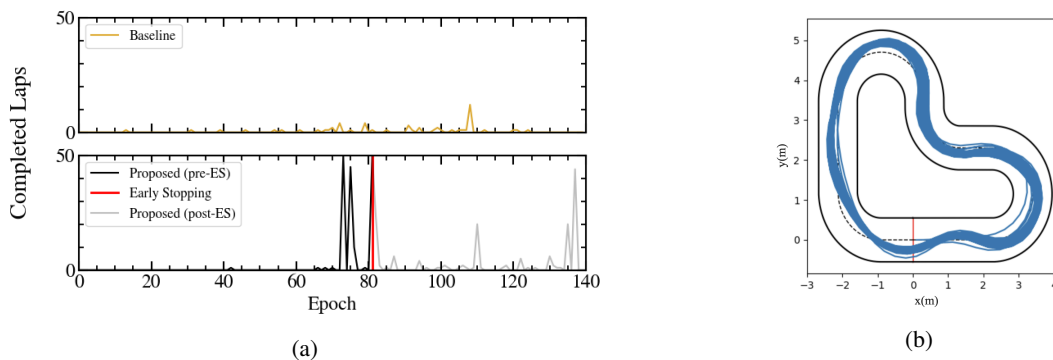


Fig. 7: **Left:** Comparison between the baseline and the proposed imitation learning objective in Experiment V-C. The setting is the same as Experiment V-B, except the controllers must rely only on image and velocity feedback instead of the full state. The tests are initialized at the same initial condition, and the rules are the same as Experiment V-B. The dotted line shows the performance in subsequent epochs if training continues. In the proposed method, $\lambda = 1$, $\rho = 0.5$. **Early stopping** (ES) is applied when a controller completes 50 laps for the second time. **Right:** Rollout of π_θ with proposed method when early stopping is triggered in Experiment V-C. The policy completed 50 consecutive laps, with the average lap time = 5.665 seconds, max lap time = 5.8 seconds, and min lap time = 5.5 seconds. In comparison, the average lap time for the expert is 4.805 seconds.

optimization landscape introduced by the evolving safety penalty term. Strategies such as adaptive hyperparameter scheduling and curriculum learning may help mitigate variance and improve reliability. Finally, while we show strong results in simulation, we expect real-world differences to degrade performance. We plan to mitigate this via robust or domain-randomized expansions of our training and by carefully validating \hat{p}_{ϕ_p} on physical systems.

REFERENCES

- [1] J. Betz et al., “Autonomous Vehicles on the Edge: A Survey on Autonomous Vehicle Racing,” *IEEE Open Journal of Intelligent Transportation Systems*, pp. 1–1, 2022.
- [2] C. Celemin et al., “Interactive Imitation Learning in Robotics: A Survey,” *arXiv.org*, Oct. 31, 2022.
- [3] L. Le Mero, D. Yi, M. Dianati, and A. Mouzakitis, “A Survey on Imitation Learning Techniques for End-to-End Autonomous Vehicles,” *IEEE Transactions on Intelligent Transportation Systems*, vol. 23, no. 9, pp. 14128–14147, Sep. 2022.
- [4] M. Zare, P. M. Kebria, A. Khosravi, and S. Nahavandi, “A Survey of Imitation Learning: Algorithms, Recent Developments, and Challenges,” *arXiv.org*, Sep. 05, 2023.
- [5] W. Sun, B. J. Andrew, and B. Boots, “Truncated Horizon Policy Search: Combining Reinforcement Learning & Imitation Learning,” *arXiv.org*, 2018.
- [6] J. Spencer, S. Choudhury, A. Venkatraman, B. Ziebart, and B. J. Andrew, “Feedback in Imitation Learning: The Three Regimes of Covariate Shift,” *arXiv.org*, 2021.
- [7] U. Rosolia and F. Borrelli, “Learning Model Predictive Control for Iterative Tasks. A Data-Driven Control Framework,” *IEEE Transactions on Automatic Control*, vol. 63, no. 7, pp. 1883–1896, Jul. 2018.
- [8] E. Garone and M. M. Nicotra, “Explicit Reference Governor for Constrained Nonlinear Systems,” *IEEE Transactions on Automatic Control*, vol. 61, no. 5, pp. 1379–1384, Sep. 2015.
- [9] S. Bansal, M. Chen, S. Herbert, and C. J. Tomlin, “Hamilton-Jacobi reachability: A brief overview and recent advances,” *IEEE Xplore*, Dec. 01, 2017.
- [10] A. D. Ames, S. Coogan, M. Egerstedt, G. Notomista, K. Sreenath, and P. Tabuada, “Control Barrier Functions: Theory and Applications,” 2019 18th European Control Conference (ECC), Jun. 2019.
- [11] Y. Pan et al., “Agile Autonomous Driving using End-to-End Deep Imitation Learning,” *arXiv.org*, 2017.
- [12] E. Kaufmann, A. Loquercio, R. Ranftl, M. Müller, V. Koltun, and D. Scaramuzza, “Deep Drone Acrobatics,” *arXiv.org*, 2020.
- [13] E. Kaufmann, L. Bauersfeld, A. Loquercio, M. Müller, V. Koltun, and D. Scaramuzza, “Champion-level drone racing using deep reinforcement learning,” *Nature*, vol. 620, no. 7976, pp. 982–987, Aug. 2023.
- [14] P. R. Wurman et al., “Outracing champion Gran Turismo drivers with deep reinforcement learning,” *Nature*, vol. 602, no. 7896, pp. 223–228, Feb. 2022.
- [15] K. P. Wabersich and M. N. Zeilinger, “A predictive safety filter for learning-based control of constrained nonlinear dynamical systems,” *arXiv.org*, 2018.
- [16] W. Lavanakul, J. J. Choi, K. Sreenath, and C. J. Tomlin, “Safety Filters for Black-Box Dynamical Systems by Learning Discriminating Hyperplanes,” *arXiv.org*, 2024.
- [17] S. Ross, G. J. Gordon, and J. A. Bagnell, “A Reduction of Imitation Learning and Structured Prediction to No-Regret Online Learning,” *arXiv.org*, Mar. 16, 2011.
- [18] Ciftci, Yusuf Umut, D. Chiu, Z. Feng, Sukhatme, Gaurav S, and S. Bansal, “SAFE-GIL: SAFETY Guided Imitation Learning for Robotic Systems,” *arXiv.org*, 2024.
- [19] M. Bojarski et al., “End to End Learning for Self-Driving Cars,” *arXiv.org*, 2016.
- [20] Y. Liu, D. Romeres, D. K. Jha, and D. Nikovski, “Understanding Multi-Modal Perception Using Behavioral Cloning for Peg-In-a-Hole Insertion Tasks,” *arXiv.org*, 2020.
- [21] L. Le Mero, D. Yi, M. Dianati, and A. Mouzakitis, “A Survey on Imitation Learning Techniques for End-to-End Autonomous Vehicles,” *IEEE Transactions on Intelligent Transportation Systems*, vol. 23, no. 9, pp. 14128–14147, Sep. 2022.
- [22] J. Zhang and K. Cho, “Query-Efficient Imitation Learning for End-to-End Autonomous Driving,” *arXiv.org*, 2016.
- [23] K. P. Wabersich et al., “Data-Driven Safety Filters: Hamilton-Jacobi Reachability, Control Barrier Functions, and Predictive Methods for Uncertain Systems,” *IEEE Control Systems*, vol. 43, no. 5, pp. 137–177, Sep. 2023.
- [24] I. Tabbara and H. Sibai, “Learning Ensembles of Vision-based Safety Control Filters,” *arXiv.org*, 2024.
- [25] R. K. Cosner, Y. Yue, and A. D. Ames, “End-to-End Imitation Learning with Safety Guarantees using Control Barrier Functions,” *arXiv.org*, 2022.
- [26] Tzanis Anevlavis and Paulo Tabuada, “Computing controlled invariant sets in two moves,” pp. 6248–6254, Dec. 2019.
- [27] A. Dosovitskiy, G. Ros, F. Codevilla, A. Lopez, and V. Koltun, “CARLA: An Open Urban Driving Simulator,” *arXiv.org*, Nov. 10, 2017.